Structural Engineering and Mechanics, Vol. 14, No. 2 (2002) 171-190
DOI: http://dx.doi.org/10.12989/sem.2002.14.2.171

Design and ultimate behavior of RC plates and shells: two case studies

Chang-Shik Min†

Department of Civil and Environmental Engineering, Dongguk University, Pil-dong 26, Chung-gu, Seoul 100-715, Korea

(Received March 29, 2001, Revised February 26, 2002, Accepted May 18, 2002)

Abstract. Two cases of design are performed for the hyperbolic paraboloid saddle shell (Lin-Scordelis saddle shell) and the hyperbolic cooling tower (Grand Gulf cooling tower) to check the design strength against a consistent design load, therefore to verify the adequacy of the design algorithm. An iterative numerical computational algorithm is developed for combined membrane and flexural forces, which is based on equilibrium consideration for the limit state of reinforcement and cracked concrete. The design algorithm is implemented in a finite element analysis computer program developed by Mahmoud and Gupta. The amount of reinforcement is then determined at the center of each element by an elastic finite element analysis with the design ultimate load. Based on ultimate nonlinear analyses performed with designed saddle shell, the analytically calculated ultimate load exceeded the design ultimate load from 7% to 34% for analyses with various magnitude of tension stiffening. For the cooling tower problem the calculated ultimate load exceeded the design ultimate load from 26% to 63% with similar types of analyses. Since the effective tension stiffening would vary over the life of the shells due to environmental factors, a degree of uncertainty seems inevitable in calculating the actual failure load by means of numerical analysis. Even though the ultimate loads are strongly dependent on the tensile properties of concrete, the calculated ultimate loads are higher than the design ultimate loads for both design cases. For the cases designed, the design algorithm gives a lower bound on the design ultimate load with respect to the lower bound theorem. This shows the adequacy of the design algorithm developed, at least for the shells studied. The presented design algorithm for the combined membrane and flexural forces can be evolved as a general design method for reinforced concrete plates and shells through further studies involving the performance of multiple designs and the analyses of differing shell configurations.

Key words: reinforcement design in plate and shell; hyperbolic paraboloid saddle shell; hyperbolic cooling tower; nonlinear inelastic behavior; finite element analysis.

1. Introduction

Shell structures mobilize geometry to activate both the membrane and flexural internal force systems to efficiently support any distributed loads applied to those structures. In current design practice for concrete shells (ACI 318-99, 1999), stresses due to design loads from elastic analysis are used to design reinforcement in shells based on point-wise limit state behavior (ACI SP-110, 1988, Gupta 1984). A possible justification for the practice -- elastic analysis and point-wise limit

† Associate Professor

design -- can be found from the lower bound theorem of plasticity, according to which the design load gives a lower bound on the true ultimate when the design is performed using stresses that are in a state of equilibrium and do not violate an appropriate yield or failure criterion (Chen 1982). A linear elastic analysis indeed provides an equilibrium state of stresses, and the same type of design procedure is also used in other reinforced concrete structures (ACI 318-99, 1999). Even though reinforced concrete is not an elastic-perfectly-plastic material as in the theorem, the validity of the present practice has been established through many years of analysis, testing, and experience for other types of structures, such as frames (Cheng 1995, Vecchio 1998).

Even though shells resist applied forces primarily through in-plane membrane action, bending is still induced in the shell. Therefore, a more rational approach to the design process is to include combined membrane forces and bending moments simultaneously. Currently, designers first perform the design with membrane forces only and later provide the reinforcement for bending in particular locations, such as near boundaries or near structural discontinuities. Design of reinforcement in plates and shells for a combined membrane and bending state of stress is a complex problem. A general solution, however, is starting to evolve (Gupta 1986, Lourenco and Figueiras 1995). Gupta developed an iterative trial-and-error design method using the Principle of Minimum Resistance by dividing the shell into two imaginary concrete layers with each orthogonally placed reinforcing layer. He offered several sample design problems on the element level. In 1995, Lourenco and Figueiras presented an automated design of reinforced concrete plates and shells in accordance with the CEB-FIP Model Code (1991). They implemented the design equations on a computer program, and performed several design examples, such as a simply supported slab and a shallow dome.

A complete iterative computational algorithm was developed (Min 1999, Cho and Min 2000) to design a plate or a shell element subjected to combined membrane forces and bending moments. The algorithm was developed on the basis of Gupta's derivation (1986). Gupta obtained the design equations only partly for the case of reinforcement required in the top and bottom layers simultaneously. Three more cases need to be developed for reinforcement required in the bottom layer only, for reinforcement required in the top layer only, and for no reinforcement required. In the design equations, the reinforcement will contribute to tension and the concrete compression struts parallel to the crack direction will contribute to compression. The reinforcement is assumed to have two orthogonal layers placed in the top and bottom surfaces with appropriate covers. Each reinforcement layer has rebars placed orthogonally in the x- and y-directions. For the concrete compression struts, the stress is assumed to be distributed uniformly in the depth of Whitney's stress block. The design algorithm is implemented in Mahmoud-Gupta's nonlinear computer program (1993).

To verify the design algorithms on the element level several experimental examples were designed (Cho and Min 2000). Nonlinear ultimate analyses were performed with the designed examples using Mahmoud-Gupta's program to show the adequacy of the design equations. If the calculated ultimate strength is higher than the ultimate strength obtained from the test, then the design method can be considered satisfactory. Since the calculated ultimate strengths are from 3% to 18% higher than the ultimate strength obtained from the test results with the exception of one case, the design method can be considered satisfactory on the element level. One model failed to converge when 91% of the ultimate load was applied due to very large deformation of the specimen.

In the present study, the adequacy of the design algorithm on the global structural level is evaluated by designing two shell structures, such as the hyperbolic paraboloid saddle shell and the hyperbolic cooling tower. The reinforcement design is based on the elastic stresses obtained from a

finite element analysis by applying the design ultimate load combinations (ACI 318-99, 1999). With these reinforcement designs, nonlinear ultimate analyses are perfomed for the shells with Mahmoud-Gupta's computer program to obtain the calculated ultimate strengths.

Mahmoud-Gupta's program was migrated to a Cray Y-MP C90 system at the supercomputer center of the Korea Institute of Science and Technology Information (KISTI) in Daejeon, Korea and then used in the present study. Mahmoud-Gupta's computer program was originally developed by Min and Gupta (1992, 1995, 1996) with a layered model and implementing vector algorithm (Min and Gupta 1995). This computer program was developed on the basis of Akbar and Gupta's (1985) work.

Mahmoud and Gupta (1993) modified the program to include the effects of geometric nonlinearity due to large displacement along with tension stiffening, to the nonlinearity of the concrete stress-strain curve, and to the possibility of two orthogonal cracks within the element. The finite element program was verified by comparing linear and nonlinear analytical results with the experimental results (Akbar and Gupta 1985, Min and Gupta 1992).

2. Design equations for combined membrane and flexural forces

A typical plate or shell element is subjected to simultaneously bending moments M_x, M_y, M_{xy} and membrane forces N_x, N_y, N_{xy} per unit length. In the ultimate limit state, the applied forces have to be in equilibrium with the tensile forces in the reinforcement, and the compressive forces in the concrete compression strut have to be parallel with the crack direction. In this limit state, concrete stress in compression is assumed to be distributed uniformly in the depth of Whitney's stress block. For simplication, the tensile strength of concrete is ignored as in the current design philosophy (ACI 318-99, 1999). A rigid-plastic behavior is assumed for the reinforcement rebars. The tension stiffening effect and the dowel action of the embadded rebars are not included. The contribution of compressed reinforcement is also ignored in the development of design equations.

It is assumed that the reinforcement consists of two orthogonal layers placed at the top surface and the bottom surface, with appropriate covers, and that each orthogonal reinforcement layer has rebars in the x- and y-directions, respectively. Therefore, the capacity of these reinforcements can be designanted as N^*_{xt}, N^*_{xb}, N^*_{yt} and N^*_{yb}, where subscripts x and y designate the directions, and t and b stand for the top and bottom layers, respectively. Fig. 1(a) shows a plate or shell element with

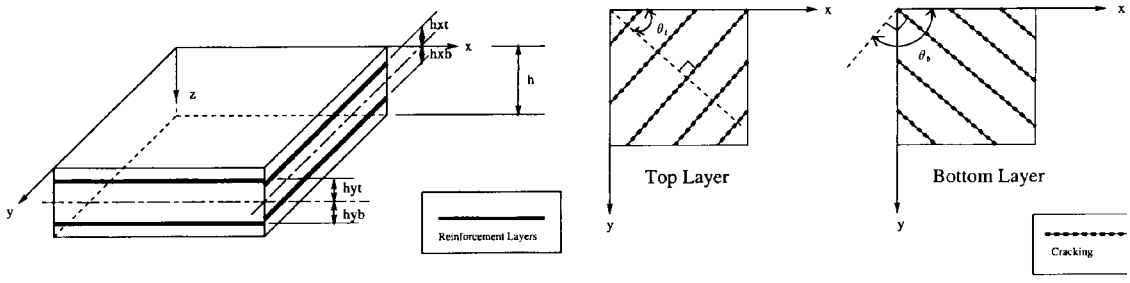

(a) Shell Element Showing the Reinforcement Layers (b) Crack Directions

Fig. 1 Four reinforcement layers (two for top and two for bottom) and crack directions

reinforcement depicted as smeared layers. At the ultimate limit state, a vertical plane of crack, whose normal makes an angle θ_t and θ_b with the x-axis in the xy plane, penetrates the top and bottom surfaces (see Fig. 1(b)). The concrete is under compression parallel to this crack; it is assumed that the depths of Whitney's stress block are a_t and a_b for the top and bottom layers, respectively. As discussed earlier, four different cases have to be considered in the design process. Only one case (reinforcement required in the top and bottom layers) is discussed here. Other cases, being similar to this, are omitted here for the sake of brevity (Min 1999).

2.1 Reinforcement required in the top and bottom layers

The total forces and moments resisted by the reinforcement in the x- and y-directions are given by

$$N_x^* = N_{xt}^* + N_{xb}^* \text{ and } N_y^* = N_{yt}^* + N_{yb}^* \tag{1}$$

$$M_x^* = -N_{xt}^* h_{xt} + N_{xb}^* h_{xb} \text{ and } M_y^* = -N_{yt}^* h_{yt} + N_{yb}^* h_{yb} \tag{2}$$

If the average compressive stress parallel to the crack direction in the concrete block is f^c, the force and moment resultants of the top and bottom concrete blocks are

$$N_t^c = -a_t f_t^c,\ M_t^c = -h_t N_t^c \text{ and } h_t = (h - a_t)/2 \tag{3}$$

$$N_b^c = -a_b f_b^c,\ M_b^c = h_b N_b^c \text{ and } h_b = (h - a_b)/2 \tag{4}$$

The resisting forces and moments given by Eqs. (1) to (4) should be under equilibrium with the applied forces and moments. Therefore, the equlibrium equations for a unit cracked element in the x- and y-directions are

$$N_x = N_x^* + N_t^c \sin^2\theta_t + N_b^c \sin^2\theta_b,\quad N_y = N_y^* + N_t^c \cos^2\theta_t + N_b^c \cos^2\theta_b \text{ and}$$
$$N_{xy} = -N_t^c \sin\theta_t \cos\theta_t - N_b^c \sin\theta_b \cos\theta_b \tag{5}$$

$$M_x = M_x^* + M_t^c \sin^2\theta_t + M_b^c \sin^2\theta_b,\quad M_y = M_y^* + M_t^c \cos^2\theta_t + M_b^c \cos^2\theta_b \text{ and}$$
$$M_{xy} = -M_t^c \sin\theta_t \cos\theta_t - M_b^c \sin\theta_b \cos\theta_b \tag{6}$$

In Eqs. (5) and (6) (six equations), we need to determine eight unknowns: four reinforcement capacities N_{xt}^*, N_{xb}^*, N_{yt}^* and N_{yb}^*; crack directions θ_t and θ_b; the depths of compressive stress block a_t and a_b. Ideally, these quantities should be selected so that the total capacity of reinforcement is the minimum possible. As discussed by Gupta (1984, 1986) and Lourenco and Figueiras (1995), the initial values of $\theta_t = \theta_b = \pm\pi/4$ give a satisfactory result with $a_t = a_b = 0.2h$. From Eqs. (3) to (6), the top and bottom concrete block resultants can be written as

$$-N_t^c = 2(h_b N_{xy} - M_{xy})/(h_c \sin 2\theta_t),\quad -N_b^c = 2(h_t N_{xy} + M_{xy})/(h_c \sin 2\theta_b)$$
$$\text{and } h_c = h - (a_t + a_b)/2 \tag{7}$$

The reinforcement capacities of top and bottom layers in the x- and y-orthogonal directions are

given with Eqs. (1) to (7) as

$$N_{xt}^{*} = N_{xt} + N_{xyt}C_{xtt}\tan\theta_t + N_{xyb}C_{xtb}\tan\theta_b \tag{8}$$

$$N_{xb}^{*} = N_{xb} + N_{xyt}C_{xbt}\tan\theta_t + N_{xyb}C_{xbb}\tan\theta_b \tag{9}$$

$$N_{yt}^{*} = N_{yt} + N_{xyt}C_{ytt}\cot\theta_t + N_{xyb}C_{ytb}\cot\theta_b \tag{10}$$

$$N_{yb}^{*} = N_{yb} + N_{xyt}C_{ybt}\cot\theta_t + N_{xyb}C_{ybb}\cot\theta_b \tag{11}$$

in which

$$N_{xt} = (h_{xb}N_x - M_x)/h_x, \quad N_{xb} = (h_{xt}N_x + M_x)/h_x, \quad N_{yt} = (h_{yb}N_y - M_y)/h_y$$
$$N_{yb} = (h_{yt}N_y + M_y)/h_y, \quad N_{xyt} = (h_bN_{xy} - M_{xy})/h_c \quad \text{and } N_{xyb} = (h_tN_{xy} + M_{xy})/h_c \tag{12}$$

and

$$C_{xtt} = (h_{xb} + h_t)/h_x, \quad C_{xtb} = (h_{xb} - h_b)/h_x, \quad C_{xbt} = (h_{xt} - h_t)/h_x, \quad C_{xbb} = (h_{xt} + h_b)/h_x$$
$$C_{ytt} = (h_{yb} + h_t)/h_y, \quad C_{ytb} = (h_{yb} - h_b)/h_y, \quad C_{ybt} = (h_{yt} - h_t)/h_y, \text{ and } C_{ybb} = (h_{yt} + h_b)/h_y \tag{13}$$

where $h_x = h_{xt} + h_{xb}$ and $h_y = h_{yt} + h_{yb}$. The compressive forces in concrete can be obtained from Eqs. (7) and (12), and are given by

$$-N_t^c = 2N_{xyt}/\sin 2\theta_t \text{ and } -N_b^c = 2N_{xyb}/\sin 2\theta_b \tag{14}$$

When the values of θ_t or θ_b are very small, then the compressive forces in Eq. (14) will be very large and the iterative numerical method will become unstable. Lourenco and Figueiras (1995) used $10^{\circ} \le (\theta_t, \theta_b) \le 80^{\circ}$ criterion for the purpose of avoiding numerical instability. Based on the numerical experiment, it was found that all the elements are converged within the maximum range of $-5^{\circ} \le (\theta_t, \theta_b) \le 5^{\circ}$. Therefore, in the present study, we set $(\theta_t, \theta_b) = 0^{\circ}$ when $|(\theta_t, \theta_b)| \le 5^{\circ}$ to avoid numerical instability. In the cases of θ_t or θ_b are set to zero, then N_{yt}^{*} and N_{yb}^{*} are equal to zero, therefore, Eq. (14) can expressed, respectively, as

$$-N_t^c = [M_y - h_{yb}N_y - (h_b - h_{yb})N_b^c\cos^2\theta_b]/(h_t + h_{yb}) \tag{15}$$

$$-N_b^c = [M_y + h_{yt}N_y + (h_t - h_{yt})N_t^c\cos^2\theta_t]/(-h_b - h_{yt}) \tag{16}$$

When the calculated values of Eqs. (8) to (11) are negative, then no reinforcement is required in that direction. One can set the reinforcement capacity of that direction to zero and recalculate the values of θ_t or θ_b. In the present study, minimum reinforcement area ($A_{s,\min}$) of ACI 318-99 (1999) is implemented for limiting crack width and spacing under the service load condition. In each direction the minimum capacity $N_{\min}^{*}$ can be obtained by multiplying the minimum reinforcement area ($A_{s,\min}$) by the yield stress of reinforcement and dividing the product by 2 as $N_{\min}^{*} = A_{s,\min}f_y/2$, where f_y is the yield stress of reinforcement. Therefore, in Eq. (8), when $N_{xt}^{*} \le N_{\min}^{*}$, then set

$N_{xt}^* = N_{\min}^*$ and calculate a new θ_t value as

$$\theta_t = \tan^{-1}(N_{\min}^* - N_{xt} - N_{xyb}C_{xtb}\tan\theta_b)/(N_{xyt}C_{xtt}) \quad (17)$$

Similarly, from Eqs. (9) to (11) if N_{xb}^*, N_{yt}^* and N_{yb}^* are smaller than $N_{\min}^*$, then set N_{xb}^*, N_{yt}^* and $N_{yb}^* = N_{\min}^*$, respectively, and obtain θ_t or θ_b values accordingly.

2.2 Design algorithm for reinforcement required in the top and bottom layers (both layers)

Step 1: Assume $a_t = a_b = 0.2$ h and $\theta_t = 45^o|N_{xyt}|/N_{xyt}$, $\theta_b = 45^o|N_{xyb}|/N_{xyb}$.

Step 2: Calculate N_{xt}^*, N_{xb}^*, N_{yt}^* and N_{yb}^* using Eqs. (8) to (11), respectively.

Step 3: If N_{xt}^*, N_{xb}^*, N_{yt}^* and $N_{yb}^* \le N_{\min}^*$; then move to "compression of both layers" case.

If N_{xt}^* and $N_{yt}^* \le N_{\min}^*$; then move to "compression of top layer" case.

If N_{xb}^* and $N_{yb}^* \le N_{\min}^*$; then move to "compression of bottom layer" case.

Step 4: (Reinforcement required in both layers)

(i) When $N_{xt}^* \le N_{\min}^*$, obtain θ_t using Eq. (17) and set $N_{xt}^* = N_{\min}^*$.

If $N_{xb}^* \le N_{\min}^*$, calculate θ_b and set $N_{xb}^* = N_{\min}^*$.

If $|\theta_t| \le$ thmin, set $N_{yt}^* = N_{\min}^*$ (set thmin = 5°); othewise obtain N_{yt}^* using Eq. (10).

If $|\theta_b| \le$ thmin; set $N_{yb}^* = N_{\min}^*$; otherwise obtain N_{yb}^* using Eq. (11).

If $N_{yb}^* \le N_{\min}^*$; then move to "compression of bottom layer" case.

If $N_{yb}^* \le N_{\min}^*$, calculate θ_b; obtain N_{xb}^* using Eq. (9) and set $N_{yb}^* = N_{\min}^*$.

If $|\theta_t| \le$ thmin; set $N_{yt}^* = N_{\min}^*$; otherwise obtain N_{yt}^* using Eq. (10).

If $N_{xb}^* \le N_{\min}^*$; then move to "compression of bottom layer" case.

Otherwise compute N_{xb}^* using Eq. (9).

If $|\theta_t| \le$ thmin; then set $N_{yt}^* = N_{\min}^*$; otherwise obtain N_{yt}^* using Eq. (10).

If $|\theta_b| \le$ thmin; then set $N_{yb}^* = N_{\min}^*$; otherwise obtain N_{yb}^* using Eq. (11).

If $N_{yt}^* \le N_{\min}^*$; then move to "compression of bottom layer" case.

(ii) When $N_{yt}^* \le N_{\min}^*$; Obtain θ_t and set $N_{yt}^* = N_{\min}^*$ [Other operations can be done similarly with Step 4(i)].

(iii) When $N_{xb}^* \le N_{\min}^*$; Obtain θ_b and set $N_{xb}^* = N_{\min}^*$ [Other operations can be done similarly with Step 4(i)].

(iv) When $N_{yb}^* \le N_{\min}^*$; Obtain θ_b and set $N_{yb}^* = N_{\min}^*$ [Other operations can be done similarly with Step 4(i)].

(v) None of the above case, then Compute N_{xt}^*, N_{xb}^*, N_{yt}^* and N_{yb}^* using Eqs. (8) to (11).

Step 5: Compute N_t^c and N_b^c using Eq. (14).

If $|\theta_t| \leq$ thmin; set $\theta_t = 0^o$ and compute N_t^c using Eq. (15).

If $|\theta_b| \leq$ thmin; set $\theta_b = 0^o$ and compute N_b^c using Eq. (16).

Step 6: Compute a_t and a_b using Eqs. (3) and (4) with the nominal compressive stress of cracked and uncracked concrete, respectively.

Step 7: Compute all the coefficients in Eqs. (12) and (13).

Step 8: Check the depth of the shell by $a_t + a_b \leq 0.85$ h (The parameter 0.85 comes from Whitney's stress block parameter. If it is not satisfied, then the shell's thickness, or the f_c' of concrete, has to be increased.)

Step 9: Check convergence by $|a_{t(i)} - a_{t(i-1)}| > conv$ or $|a_{b(i)} - a_{b(i-1)}| > conv$; then go to Step 2 (Set equal to $conv = 0.0001$ h).

Step 10: Compute steel area per unit length by $A_{s(xt, xb, yt, yb)} = (N_{xt}^*, N_{xb}^*, N_{yt}^*, N_{yb}^*)/f_y$.

3. Saddle shell problem: Analysis model and methods

The design of reinforced concrete shells requires careful attention to all the parameters affecting their behavior. Some of these parameters for the hyperbolic paraboloid shells, such as rise-span ratio, edge beam type and eccentricity, and supporting system type, have been extensively studied from both a theoretical and an experimental point of view (ACI SP-110, 1988). The focus here is on designing the reinforcement for combining membrane and flexural forces for the shell and evaluating the adequacy of the design algorithm based on the ultimate behavior of the designed shell. The geometry and the material properties of the Lin-Scordelis saddle shell (Lin and Scordelis 1975) are used in the present design without any possible improvement for the design, which has also used by numerous research teams in the past, such as Muller and Scordelis (1977), Akbar and Gupta (1985), Min and Gupta (1992, 1994), Min (1997a, 1997b, 1999) and Noh (1999).

The edge beams and the shell are modeled by the same four-node shell element. The shell elements are divided into ten concrete layers and two reinforcement layers, with both direction reinforcements placed near the surface of the shell with proper cover. One quarter of the shell (divided by the orthogonal diagonal) needs to be analyzed by recognizing two planes of mirror reflection symmetry and by applying appropriate constraint equations with four-node bilinear elements (Min and Gupta 1992). Considering the previous mesh convergence study (Min and Gupta 1992, 1994), the most refined model, 64-by-64 mesh (element size = 0.38 m × 0.38 m), is used in the present study. The formula $(1.4D + 1.7L)/0.9$ is used in accordance with ACI 318-99 (1999), in which D represents the dead loads of the shell and the edge beams and L due to the live loads. The formula $(1.4D + 1.7L)/0.9$ is called the ultimate design load. As with Muller and Scordelis (1977), the snow load of 957.6 Pa. (20 psf.) is applied for the design as live load on the saddle shell. The strength reduction factor 0.9 is used in the present design, which is recommended by ACI. Since there is no direct way of representing the reduction of capacity as far as the analysis is concerned, it is assumed that the design strength of the shell is $(1.4D + 1.7L)/0.9$. Fractions of the displacement are applied proportionally at the tip of the shell (see Fig. 2). A fraction of displacement will be converted to a set of applied load in the analysis (Min and Gupta 1992). The objective of applying the loads in this manner is to check the design strength against a consistent combination of factored

dead and live loads. If the design method is safe, the ultimate load predicted by the analysis should be 100% or more of the ultimate design load. Based on the previous study (Min and Gupta 1992), the performance of the edge beams is more than satisfactory. Therefore, the edge beam of Lin-Scordelis saddle shell is used without developing any rational design method.

3.1 Design and ultimate behavior

The shell is first analyzed elastically for the ultimate design load, and the required reinforcement ratios in each element are obtained at the center integration point. The shell thickness of 10.2 cm (4 in) is used in the design as in Lin and Scordelis (1975). Design parameters used in the design are as follows (Muller and Scordelis 1977, Min and Gupta 1992): (1) Nominal compressive strength parallel to the crack is taken as $0.4f_c'$ = 8.27 MPa (ACI 318-99, 1999); (2) The yield stress of the reinforcement is taken as 414 MPa (60 ksi); (3) With proper cover 1.27 cm (0.5 in), the top and bottom reinforcement layers are placed orthogonally at 3.8 cm (1.5 in) from the mid-surface of the section (Since the total shell thickness is 10.2 cm, we may choose welded wire fabric as the

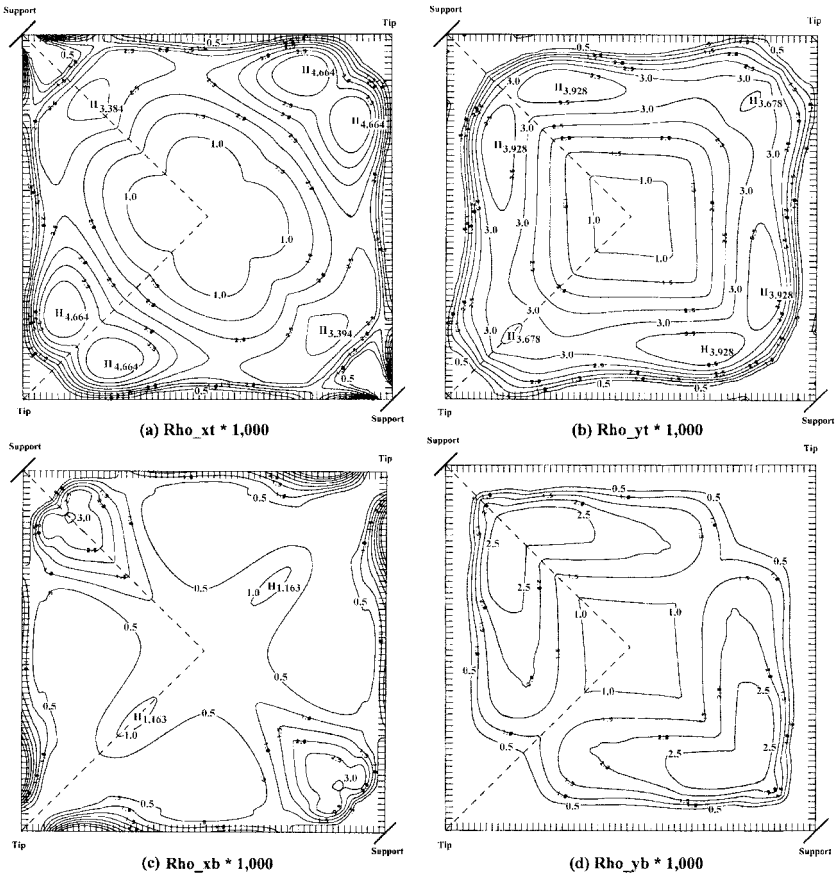

Fig. 2 Distribution of the required reinforcement ratios: Upper layer (a) Rho_xt (x-dir.) and (b) Rho_yt (y-dir.); Lower layer (c) Rho_xb (x-dir.) and (d) Rho_yb (y-dir.)

reinforcement.); and (4) The minimum reinforcement ratio is set to 0.025%, which is about 1/10 of the usual minimum reinforcement ratio used in practice. Thus 0.0125% of reinforcement will be provided for each direction of the layer. By reducing the minimum reinforcement ratio by about 1/10, any dependence on the ultimate strength by the minimum reinforcement ratio can be eliminated.

Fig. 2 shows the distribution of the required reinforcement ratios obtained by the present design algorithm. The reinforcement ratios are generally greater than the minimum reinforcement ratio except near the tip and the support and alongside the edge beams. Figs. 2(a) and (b) show that the contours for the upper layer are more complicated than those of the lower layers (Figs. 2(c) and (d)). For the upper layer in the *x*-direction (see Fig. 2(a)), the peak reinforcement ratio occurs near the tip parallel to the support-to-support diagonal by 0.466% and another peak is near the support with 0.339% of reinforcement ratio. For the *y*-direction of the upper layer (see Fig. 2(b)) the peak reinforcement ratio occurs elsewhere near the support by 0.393%, and another peak is near the tip with 0.368% of reinforcement ratio. On the other hand, data for the lower layer in the *x*-direction, Fig. 2(c) shows that the peak occurs near the support on the diagonal line by 0.3% and for most of the shell a relatively uniform reinforcement ratio of 0.05% is required. For the *y*-direction in the lower layer, the 0.25% of peak ratio areas occur near the support, and the reinforcement ratio for the shell is in the range of a ratio of 0.1% to 0.25% (see Fig. 2(d)).

In reality, it would be impractical to vary the steel distribution from element to element. Since the purpose of the present study is to evaluate the theoretical capacity of the shell based on the design algorithm, the reinforcement ratios calculated for each element are used without any effort to select real reinforcing bars. In a practical design, the actual reinforcement would generally be greater than the calculated value since more uniform reinforcement would be required.

Table 1 shows a comparion of the design methods and the total reinforcement amount required by the various research teams. Compared with the previous design based on the membrane forces only (Min 1997b), the design algorithm requires 6% and 2% increases in the total amount of reinforcement for the *x*- and *y*-directions, respectively. Considering combined membrane and flexural forces in the design, it could be expected that the design would require somewhat more

Table 1 Total amount of reinforcement required for the Lin-Scordelis saddle shell by the various design methods

	Design methods	Total amount of reinforcement required (unit = m^3)	
		x-dir.	*y*-dir.
Muller-Scordelis (1977)	· Use Nxy only-membrane analysis · Elastic design method	Each direction: 0.253 (reinforcement ratio=0.42%)	
Min-Gupta (1994)	· Use Nxy only-membrane analysis · Limit state design method	Each direction: 0.155 (reinforcement ratio=0.257%)	
Min (1997b)	· Elastic finite element analysis · Use N_x, N_y, and N_{xy} only · Limit state design method	0.161	0.189
Present study	· Elastic finite element analysis · Use membrane and flexural forces · Design algorithm developed	0.171	0.192

reinforcement than the design for membrane forces only. The reinforcement increase is quite moderate. There is also a contrast between the reinforcement required for the upper and lower layers. In the *x*-direction the upper layer requires 2.5 times more reinforcement than the lower layer (the upper layer consists of 71% of the total reinforcement and the lower consists of 29%). In the *y*-direction the upper layer requires 1.7 times more reinforcement than the lower layer (the upper layer consists of 63% of the total reinforcement and the lower consists of 37%). Requiring 1.7 times to 2.5 times more reinforcement in the upper layer than in the lower layer indicates that very significant bending action is developed in the saddle shell. Moreover, complicated contour lines in the upper layers also indicate considerable bending action in the shell (see Fig. 2).

3.2 Load-deflection curves

Mahmoud and Gupta (1993) modeled tension stiffening as a gradual unloading of the concrete stress-strain curves in tension. The parameter γ is the ratio of the strain at which the tensile strength of concrete becomes zero and the cracking strain of concrete. Thus, a γ of unity means no tension stiffening. The tension stiffening effect is a complex phenomenon and is dependent on many factors, such as steel percentage, reinforcing bar diameter, bond stress, concrete strength, and reinforcement distribution. As discussed by Milford and Schnobrich (1984) and Mahmoud and Gupta (1993), there is still little experimental data available on which to base the quantification of tension stiffening and the rational modeling of the tension stiffening effect in a finite element analysis. Since the tensile properties of concrete would vary over the life of a shell, predicting the effect of tension stiffening in reinforced concrete is possible with the implied limitation. Therefore, in the present study we performed ultimate analyses with tension stiffening parameters of γ = 5~20.

Fig. 3 shows the load-deflection curves for the saddle shell with tension stiffening parameter, γ = 5, 10, 15 and 20. The load-deflection curves are quite straight until it reaches the unconverged step. As observed by the previous study (Min 1997a), the actual load-deflection curve goes down after it reaches the final converged loading step. Similar observations were made by Muller and Scordelis (1977). For the γ = 5 case, at the last converged loading step 32 the analysis reaches the convergence with 107% of the estimated ultimate load and a 9.5 cm vertical tip displacement. At the

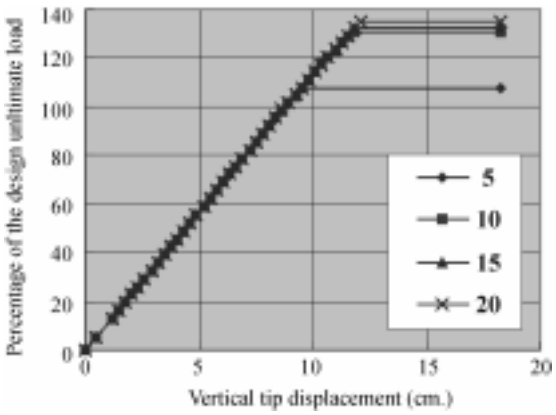

Fig. 3 Load-deflection curves for the saddle shell with tension stiffening parameters of from 5 to 20

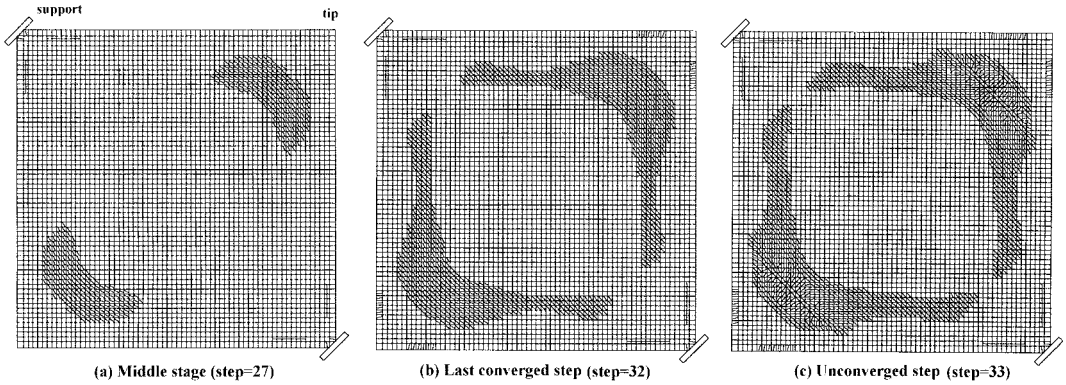

Fig. 4 Crack development on the top concrete layer for the tension stiffening parameter 5

next loading step, the saddle shell failed to make a convergence and the load-deflection curve goes down. The failure is initiated by a formation of failure lines near the tip in a direction parallel to the support-to-support diagonal (a cantilever type failure), and consequently large residual forces are found in those areas (see Fig. 4(c)). No yielding of reinforcement is observed up to the last converged loading step, and increasing the steel yield stress did not prevent or delay the formation of the failure lines on the concrete layers. Large unbalanced forces were created by the formation of triangular-shape edge failure areas. The ultimate design load at the last converged loading step is considered to be the calculated ultimate load for the shell.

Increasing tension stiffening parameter to 10, the formation of the failure lines is delayed due to an increase in concrete strength after cracking, and consequently the calculated ultimate load is increased to 131% of the design load combination with the vertical tip displacement of 11.8 cm. Additional increasing of tension stiffening parameters to 15 and 20 has little effect on the calculated ultimate loads. It increases the calculated ultimate load only 1% and 3% from the tension stiffening parameter 10 case, respectively.

3.3 Crack patterns

Fig. 4 shows the progressive development of cracks on the top concrete layer until the unconverged step 33 for the $\gamma = 5$ case. Near the tip regions the cracks start to develop on the top concrete layer when 72.1% of the design ultimate load is applied. As the applied load is increased, the cracks in those regions are expanded to form crescent shapes (see Fig. 4(a)). At the last converged step (step 32) the cracking area expanded to the entire shell surface like a ring (see Fig. 4(b)). These cracks penetrate only to the 4^{th} concrete layer from the top at the ultimate, which indicates that they are formed primarily because of bending action. The crack directions in those regions are mainly parallel to the support-to-support diagonal, indicating that the shell acts globally like two cantilevers supported by the line of support-to-support diagonal. At the bottom concrete layer no major cracks are developed except those along the edge beams, which are formed at an early loading step. They have little effect on the global behavior of the saddle shell.

Fig. 4(c) clearly shows a formation of failure lines parallel to the support-to-support diagonal, which is formed about 6.84 m (22.39 ft) from the tip of the shell to the direction of perpendicular

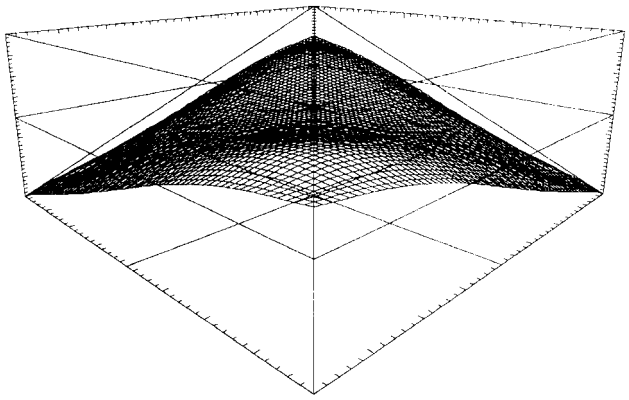

Fig. 5 Deformed shape of the saddle shell at the ultimate with tension stiffening parameter of 5 (magnification factor =30)

for the support-to-support diagonal. Muller and Scordelis (1977) shows similar failure lines, called "yield lines", in the range of 6.46~8.62 m from the tip of the shell. Fig. 5 shows a deformed shape of the saddle shell at the last converged loading step with tension stiffening parameter 5. A formation of failure lines near the tip parallel to the support-to-support is clearly shown in Fig. 5 by bending the tip area significantly. The failure lines formed on the concrete layers generate large unbalanced forces and finally lead to a failure of the shell. In the edge beams, Fig. 4(b) shows this small cracking area near the tip of the shell. Only on the top concrete layer do those cracks develop, indicating the edge beams acted as compression flanges with a negative moment on the cantilever (ACI SP-110, 1988). These cracks do not significantly affect the stiffness of the shell until the failure (see Fig. 3). After cracking, the behavior of the shell is mainly controlled by the tension stiffening effect, not by steel yield stress as indicated by the current design philosophy.

3.4 Discussion

A hyperbolic paraboloid saddle shell (Lin-Scordelis saddle shell) is designed to check the design strength against a consistent design load, therefore to verify the adequacy of the design algorithm developed. The amount of reinforcement is determined at the center of each element, which was obtained from an elastic finite element analysis by applying the design ultimate load combination, $(1.4D + 1.7L)/0.9$. Based on the nonlinear ultimate analyses performed, the analytically calculated ultimate load exceeded the design ultimate load from 7% to 34% for analyses with tension stiffening parameters of from 5 to 20. Observing the crack patterns at the ultimate, the shell shows that it resists not only through membrane action, but also by bending action. Therefore, designing the HP saddle shell with combined membrane and flexural forces is indispensable. Since the tensile properties of concrete would vary over the life of the saddle shell, it is not possible to predict its ultimate strength with complete certainty. However, for the saddle shell studied, the design method gives a lower bound on the ultimate load with respect to the lower bound theorem.

4. Cooling tower problem: Analysis model and methods

Natural draught cooling towers are an effective and economical choice among all technical solutions for the prevention of thermal pollution of natural water resources caused by heated cooling water in various industrial facilities. Cooling towers are shells of double curvature that resist applied forces primarily through in-plane membrane action. The shells can be more than 150 m in height and 60 m in base diameter. The towers have a wall thickness of approximately 20~25 cm for most of the shell. The conventional approach to designing a cooling tower shell is based on the membrane stresses only and ignores bending stresses. The reasons are twofold: no general satisfactory solution exists, and it is also believed that bending plays a secondary role for such shells. Membrane stresses are usually obtained by performing a numerical elastic analysis for the design loads with a finite element computer program. Reinforcement is then proportioned using a point-wise limit design method (ACI 318-99, 1999, ACI-ASCE, 1984, Gupta 1978, 1984). Usually the reinforcement is provided in the meridional and the circumferential directions for the cooling tower.

The cooling tower designed for the Grand Gulf Nuclear Power Station, Port Gibson, Mississippi (Zurn Ind. 1977) was studied by many researchers before, such as Mang *et al*. (1983), Milford and Schnobrich (1984), Min and Gupta (1993), Mahmoud and Gupta (1993), and Choi and Noh (2000). The same cooling tower is used in this study. The same geometry and the material properties of the Grand Gulf Cooling Tower were used without any possible improvement for the design. The adequacy of the design method is evaluated by performing a nonlinear ultimate analysis using Mahmoud-Gupta's computer program (Mahmoud and Gupta 1993). Because of the symmetry of the wind load about the windward meridian and the axisymmetry of the cooling tower geometry, only one-half of the cooling tower requires analysis. The half-circumference of the tower is discretized into 24 and 18 elements in the circumferential and meridional directions, respectively. The choice of the mesh size is based on Min and Gupta's (1992) convergence study, in which analysis using a 24-by-18 model gives sufficiently accurate results compared to the results of the more refined 36-by-36

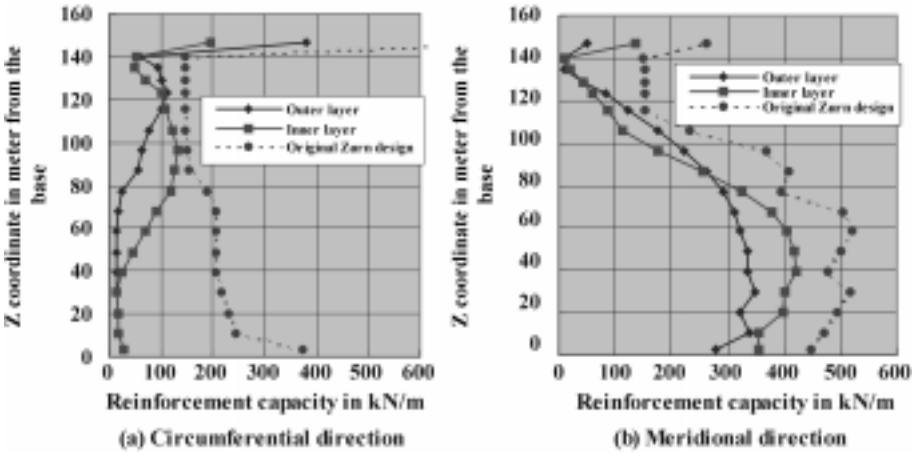

Fig. 6 Reinforcement designs by the present study and Zurn's original design

model. The shell and the ring beams are modeled by the same four-node bilinear shell element.

The formula $(0.9D + 1.3W)/0.9$ is used in accordance with ACI 318-99 (1999) and is called the ultimate design load. The wind load (W) recommended in the ACI-ASCE Committee 334 report (1984) is used for the circumferential variation and the vertical wind-pressure distribution of the loading. A reference wind speed (V_{f30}) of 145 km/h (90 Mph) for a 100-year return period was used. In the ultimate state analysis, fractions of the displacement are applied proportionally at the throat of the tower to check the design strength against a consistent combination of factored loads. A fraction of applied displacement will be converted to a set of applied load in the analysis (Min and Gupta 1992).

4.1 Design and ultimate behavior

The tower was first analyzed elastically for the ultimate design load, and the required reinforcement ratios [the two meridional layers (outer and inner layers) and the two circumferential layers] were obtained by choosing the maximum capacity of all the corresponding values calculated around the circumference at any height. Design parameters used in the design are as follows (Min and Gupta 1992, 1993): (1) Nominal compressive strength parallel to the crack is taken as $0.4f_c' = 8.27$ MPa; (2) Nominal compressive stress of concrete in the compression zone is taken as $0.85f_c' = 0.85 \times 20.68 = 17.6$ MPa; (3) The yield stress of the reinforcement is taken as 414 MPa (60 ksi); (4) As with Zurn's original design, 3.8 cm (1.5 in) of concrete cover was assumed for the entire tower; and (5) The minimum reinforcement ratio is set at 0.025%, which is about 1/10 of the usual minimum reinforcement ratio used in practice.

Fig. 6 shows the distribution of the required reinforcement capacity obtained by the present design algorithm and Zurn's original design. Fig. 6(a) shows that about 40 to 140 m of the tower from the base the required reinforcement capacity for the outer and inner circumferential layers exhibits discrepancies, and the maximum discrepancy occurred around 68 m from the base by 5.72 times more reinforcement required for the inner layer than the outer layer. The discrepancies indicate that the tower developed a great deal of bending action in this direction to resist applied loads. For the meridional direction, a similar observation can be made from Fig. 6(b), at about 10 to 120 m from the base of the tower. Bending action in the meridional direction also occurred, even though

Table 2 Comparison of the total amount of reinforcement capacities required from Zurn's original design and the present design algorithm

Design methods		Total amount of reinforcement capacity required (unit = MN/m)			
		Circumferential dir.		Meridional dir.	
		Outer layer	Inner layer	Outer layer	Inner layer
Zurn Ind. deisgn (1977)	· Elastic finite element analysis · Use N_x, N_y, and N_{xy} only · Limit state design method	4.07		6.35	
Present study	· Elastic finite element analysis · Use membrane-flexural forces · Design algorithm developed	1.21 (30%)*	1.38 (34%)	4.35 (69%)	3.86 (61%)

*Percentage of the layer compared to the capacity of Zurn's original design

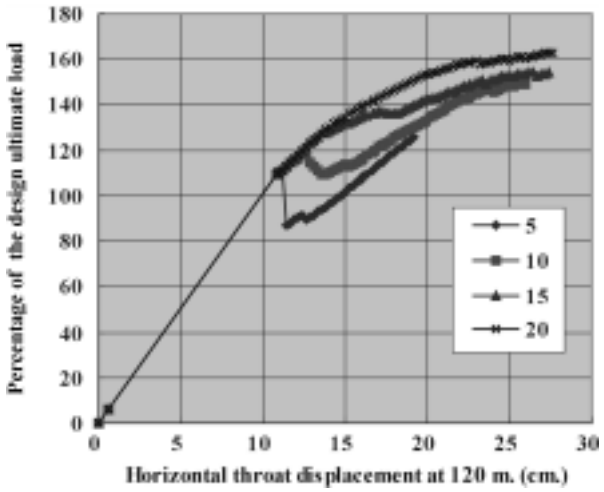

Fig. 7 Load and throat-displacement curves for the cooling tower with tension stiffening parameters of from 5 to 20

somewhat less significantly compared to the bending action in the circumferential direction. The maximum discrepancy occurred at 106 m from the base by 1.53 times more reinforcement required for the outer layer than the inner layer.

Fig. 6 also shows the Zurn Ind. design obtained from the original drawings. Zurn's design was performed by the point-wise limit state design equations considering only membrane forces (Gupta 1978, 1984). Since Zurn's design was rounded up for placing the actual bar size used and since typically in the design process the reinforcement is provided uniformly in one area, the reinforcement capacity of Fig. 6 was greater than the actual calculated design capacity. The reinforcement capacities provided by Zurn's design are well covered the reinforcement capacities required by the present study in both directions, particularly in the circumferential direction.

Table 2 shows a comparison of the total amount of reinforcement capacities required for Zurn's original design and the present study. The present design method requires only 30% (outer layer) and 34% (inner layer) of the total amount of reinforcement capacity compared to Zurn's original 4.07 MN/m total reinforcement capacity in the circumferential direction. In the meridional direction 69% and 61% are required for the outer and inner layers, respectively, compared to the 6.35 MN/m provided in Zurn's original design.

4.2 Load-deflection curves

In the finite element analysis each element is divided into 10 concrete and four steel layers. To compensate for the presence of the reinforcing steel, the concrete cross-section area is not reduced. As before, the tension stiffening parameter of γ = 5~20 is used in the nonlinear analyses. Fig. 7 shows the load and throat-displacement curves obtained by the nonlinear ultimate analyses for the tension stiffening parameters, γ = 5, 10, 15 and 20.

For the γ = 5 case, the tower shows that in an earlier loading step the load-deflection curve reaches 111% of the design ultimate load with 11.2 cm throat displacement. After that loading step the tower loses stiffness rather suddenly and the curve goes down to 87% of the design ultimate

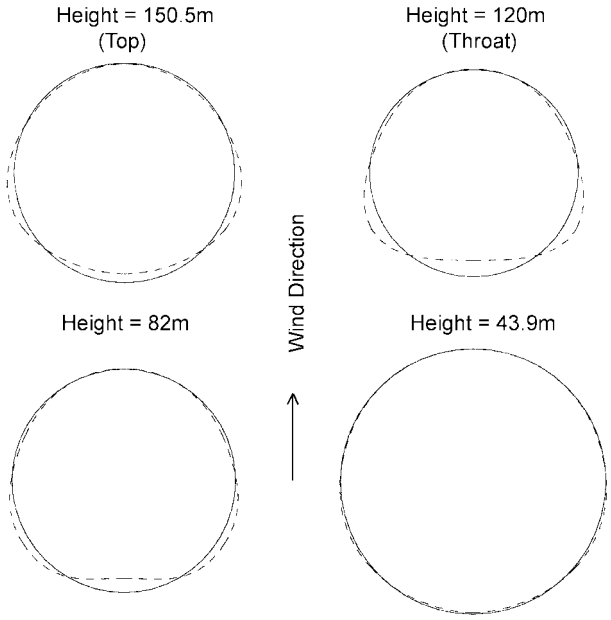

Fig. 8 Deformed shapes at the ultimate state with tension stiffening parameter of 5 : Sliced view (magnification factor = 30)

load. When the throat displacement is increased, the tower regains strength and finally reaches 126% of the design ultimate load by loading step 38 with a 19.2 cm horizontal throat displacement. At the next loading step, the tower fails to reach a convergence with large unbalanced forces in the vicinity of the throat at the windward meridian. Yielding of reinforcement is observed in the meridional direction (outer layer) of element number 145 (seventh element from the bottom at the windward meridian) just before the final converged step (step 37). At the next loading step, number 38 (the last converged step), the yielding area is not expanded to other layers or elements. To weigh the effect of the yielding of the reinforcement on the ultimate behavior of the tower, a numerical experimentation is conducted such that steel yielding is prevented in the nonlinear analysis. As observed by Mahmoud and Gupta (1993) with the original Grand Gulf cooling tower, preventing steel yielding does not change either the behavior of the tower or the calculated ultimate load.

Observing the sliced deformed shapes of the tower at the ultimate state in Fig. 8, we see that the maximum displacements occur near the throat level. Fig. 8 shows very obviously that the tower tends to buckle in the direction of the circumference. Therefore, this circumferential buckling of tower around the throat area leads eventually to a failure of the tower. The ultimate load at the last converged step is considered to be the calculated ultimate load for the shell.

When the tension stiffening parameter was increased to 10, somewhat less obvious but similar stiffness changes could be observed when the tower reached 118% of the design ultimate load with a 12.6 cm horizontal throat displacement. The tower loses stiffness after it reaches 110% with a 13.8 cm throat displacement, but the tower regains 149% - 26.0 cm (design ultimate load - throat displacement) at the last converged step. The failure mode is unchanged with the case of $\gamma = 5$. As tension stiffening parameters increases to 15 and 20, large stiffness changes are no longer observed and the tower withstands at the ultimate state by 154% - 27.4 cm and 163% - 27.6 cm, respectively.

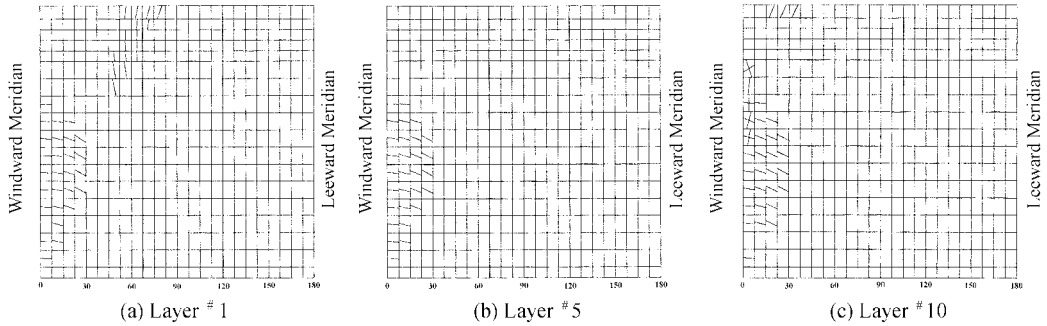

Fig. 9 Crack patterns at the ultimate on the outside surface (layer #1), middle section (layer #5) and inside surface (layer #10) with tension stiffening parameter of 20

The calculated ultimate loads are increased 3.4% and 9.4% from the tension stiffening parameter 10 case for tension stiffening parameters 15 and 20 cases, respectively.

4.3 Crack patterns

Fig. 9 shows the crack patterns on the outside surface [Fig. 9(a), layer #1], the middle section [Fig. 9(b), layer #5], and the inside surface [Fig. 9(c), layer #10] concrete layers for the tension stiffening parameter 20 case at the ultimate state. The cracks formed in the elements close to the windward meridian are relatively horizontal, while the cracks formed in the elements away from the windward meridian become slightly inclined (about 15^o with respect to the meridional direction). The cracks in this area (at circumferential angles less than 30^o and below the throat of the shell) are mainly membrane through cracks. On the other hand, above the throat of the shell at circumferential angles around 45^o to 90^o, the cracks are formed mainly due to the bending deformations [see Fig. 9(a)]; and with the exception of the cracks at the top ring beam, they penetrate to the 1^{st} layer only. In the very early loading step (step 3), initial cracks are developed on one 7^{th} strip element (located at 53.3~63.1 m from the base) at the windward meridian, and the crack is formed as through cracks. Fig. 9(c) shows that a series of cracks practically parallel to the meridian is observed under the throat of the tower at the inner surface (10^{th} layer) of the concrete layer, indicating that the tower was deformed like a ring punched at the windward meridian. These cracking patterns are conformed well to the sliced deformed shape of Fig. 8. Again, the failure mode of the tower results from the local circumferential buckling of the tower below the throat region initiated by the loss of circumferential bending capability of the tower.

4.4 Discussion

Based on the nonlinear inelastic analyses performed using Mahmoud-Gupta's computer program, the analytically calculated ultimate load exceeded the design ultimate load from 26% to 63% for an analysis with tension stiffening parameters of from 5 to 20. The failure mode for this tower is the buckling of the tower triggered by the loss of circumferential bending capabilities through the reduction of stiffness due to concrete cracking below the throat region. Yielding of the reinforcement was observed on an element at the windward meridian in the meridional direction

with a tension stiffening parameter of 5, but this has no effect on the ultimate behavior of the tower. Although it has an undesirable failure mode, the cooling tower designed in the present study is at least safe within the assumed design ultimate load.

Due to the environmental factors, the actual effective values of concrete tensile characteristics such as effective tension stiffening (after cracking) may vary significantly during the life of a tower, thus making the prediction of the realistic buckling load difficult. Furthermore, buckling is not the intended mode of failure in the present design philosophy. Therefore, further research is needed to develop simple methods of predicting the buckling load of cooling towers, which can then be used by the designers to avoid a buckling failure.

On the other hand, the environmental protection of such shells is essential for maintaining their expected ultimate strength of the shell in the long term, thus preventing any deteriorating tensile properties in the concrete. This may be achieved by coating or painting the surface of the shell.

5. Conclusions

Two cases of design are performed for the hyperbolic paraboloid saddle shell (Lin-Scordelis saddle shell) and the hyperbolic cooling tower (Grand Gulf cooling tower) to check the design strength against a consistent design load, therefore to verify the adequacy of the design algorithm. An iterative numerical computational algorithm is developed, which is based on equilibrium consideration for the limit state of reinforcement for tension and cracked concrete for compression. The design algorithm is implemented in a finite element analysis computer program developed by Mahmoud and Gupta. The amount of reinforcement is then determined at the center of each element by an elastic finite element analysis for the design ultimate load.

For the saddle shell problem, the amount of reinforcement is determined by applying the design ultimate load combination, $(1.4D + 1.7L)/0.9$. Based on the nonlinear ultimate analyses performed, the analytically calculated ultimate load exceeded the design ultimate load from 7% to 34% for analyses with tension stiffening parameters of from 5 to 20. Observing the ultimate behavior, the shell shows that it resists not only through both membrane and bending actions. Therefore, designing the saddle shell with combined membrane and flexural forces is indispensable. Since the tensile properties of concrete would vary over the life of a saddle shell, it is not possible to predict ultimate strength with complete certainty. However, for the saddle shell studied the design method gives a lower bound on the ultimate load with respect to lower bound theorem.

For the cooling tower problem, the formula $(0.9D + 1.3W)/0.9$ is used in the design for the reinforcement of the two meridional layers and the two circumferential layers. Based on the nonlinear inelastic analyses performed, the analytically calculated ultimate load exceeded the design ultimate load from 26% to 63% for an analysis with tension stiffening parameters of from 5 to 20. The failure mode for the tower designed is the buckling of the tower triggered by the loss of circumferential bending capabilities through the reduction of stiffness due to concrete cracking below the throat region. Yielding of reinforcement was observed on an element in the meridional direction at the windward meridian, but this has no effect on the ultimate behavior of the tower.

Although it has an undesirable failure mode, the cooling tower designed in the present study is at least safe within the assumed design ultimate load. Due to environmental factors, the actual effective values of concrete tensile characteristics, such as effective tension stiffening, may vary during the life of a tower, thus making the prediction of the realistic buckling load difficult. Furthermore,

buckling is not the intended mode of failure in the present design philosophy. Therefore, further research is needed to develop simple methods of predicting the buckling load of cooling towers, which can then be used by the designers to avoid a buckling failure.

Even though the ultimate loads are strongly dependent on the tensile properties of concrete, the calculated ultimate loads are higher than the design ultimate loads for both design cases. For the cases studied, the design algorithm gives a lower bound on the design ultimate load with respect to the lower bound theorem. This shows the adequacy of the design algorithm developed, at least for the shells studied. The presented design algorithm for combined membrane and flexural forces can be evolved as a general design method for reinforced concrete plates and shells through further studies involving the performance of multiple designs and analyses of different shell configurations.

References

ACI 318-99. (1999), "Building code requirements for reinforced concrete and commentary (ACI 318R-99)", American Concrete Institute, P.O. Box 9094, Farmington Hills, MI 48333.

ACI SP-110. (1988), "Hyperbolic paraboloid shells: state of the art", American Concrete Institute, Prepared by ACI Committee 334 - *Joint ACI-ASCE, SP-110*, 1988.

ACI-ASCE. (1984), "Reinforced concrete cooling tower shells - practice and commentary", *ACI J.*, Nov.-Dec. ACI-ASCE Comm. 334, Title No. 81-52.

Akbar, H. and Gupta, A.K. (1985), "Membrane reinforcement in concrete shells: design versus nonlinear behavior", *Reinf. Concrete Shell Res. Rep.*, North Carolina State Univ., Raleigh, NC 27695-7908.

CEB-FIP Model Code. (1991), Comite Euro-International du Beton, Final Draft, Bull. d'Inform., 203, 204, 205.

Chen, W.F. (1982), *Plasticity in Reinforced Concrete*, McGraw-Hill Book Company, 474 pp.

Cheng, Y.M. (1995), "Finite element modeling of reinforced concrete structures with laboratory verification", *Struct. Engrg. and Mech.*, **3**(6), 593-609.

Cho, H.J. and Min, C.S. (2000), "Combined membrane and flexural reinforcement in plates and shells", *J. Korean Society of Civil Engineers*, **29**(5-A), 725-735 (in Korean).

Choi, C.-K. and Noh, H.-C. (2000), "Stochastic analysis of shape imperfection in RC cooling tower shells", *J. Struct. Engrg.*, ASCE, **126**(3), 417-423.

Gupta, A.K. (1978), "Grand gulf cooling tower study", *Tech. Rep.*, IIT Res. Inst., Chicago, Illinois, Dec. Proj. J8325/Rep. No. 78J063.

Gupta, A.K. (1984), "Membrane reinforcement in concrete shells: a review", *Nuclear Engrg. Design*, **82**, 63-75.

Gupta, A.K. (1986), "Combined membrane and flexural reinforcement in plates and shells", *J. Struct. Div.*, ASCE, **112**(3), 550-557.

Lourenco, P.B. and Figueiras, J.A. (1995), "Solution for the design of reinforcement concrete plates and shells", *J. Struct. Engrg.*, ASCE, **121**(5), 815-823.

Lin, C.S. and Scordelis, A.C. (1975), "Nonlinear analysis of RC shells of general form", *J. Struct. Div.*, ASCE, **101**(3), 523-538.

Mahmoud, B.E.H. and Gupta, A.K. (1993), "Inelastic large displacement behavior and buckling of hyperbolic cooling tower shells", *Tech. Rep.*, NCSU, Raleigh, NC.

Mang, H.A., Floegl, H., Trappel, F. and Walter, H. (1983), "Wind-loaded reinforced-concrete cooling towers: buckling or ultimate load?", *Engrg. Struct.*, **5**, 163-180.

Milford, R.V. and Schnobrich, W.C. (1984), "Nonlinear behavior of reinforced concrete cooling towers", *Tech. Rep*. Univ. of Illinois, Urbana-Champaign, IL 61801, Struct. Res. Series No. 514.

Min, C.S. and Gupta, A.K. (1992), "A study of inelastic behavior of reinforced concrete shells using supercomputers", *Tech. Rep.*, NCSU, Raleigh, NC.

Min, C.S. and Gupta, A.K. (1993), "Inelastic behavior of hyperbolic cooling tower", *J. Struct. Engrg.*, ASCE, **119**(7), 2235-2255.

Min, C.S. and Gupta, A.K. (1994), "Inelastic behavior of reinforced concrete hyperbolic paraboloid saddle shell",

Engrg. Struct., **16**(4), 227-237.
Min, C.S. and Gupta, A.K. (1995), "Vector algorithm for layered reinforced concrete shell element stiffness matrix", *Struct. Engrg. and Mech.*, **3**(2), 172-183.
Min, C.S. and Gupta, A.K. (1996), "Inelastic vector finite element analysis of RC shells", *Struct. Engrg. and Mech.*, **4**(2), 139-148.
Min, C.S. (1997a), "Ultimate behavior of RC hyperbolic paraboloid saddle shell", *Struct. Engrg. and Mech.*, **5**(5), 507-512.
Min, C.S. (1997b), "Design versus nonlinear behavior of RC hyperbolic paraboloid saddle shell", *J. Korean Society of Civil Engineers*, **17**(I-6), 935-945 (in Korean).
Min, C.S. (1999), "Design of RC plates and shells subjected to membrane force and flexural moment", *J. Korean Society of Civil Engineers*, **19**(I-2), 171-183 (in Korean).
Muller, G. and Scordelis, A.C. (1977), "Nonlinear analysis of reinforced concrete hyperbolic paraboloid shells", *Tech. Rep.*, University of California, Berkeley, California 94720, October, Report No. UC-SESM 77-6.
Noh, H.C. (1999), "Wind induced nonlinear behavior of reinforced concrete hyperbolic shell with shape imperfection", Ph.D. Thesis, Civil Engrg. Dept., Korea Advanced Institute of Science & Technology.
Vecchio, F.J. (1998), "Lessons from the analysis of a 3-D concrete shear wall", *Struct. Engrg. and Mech.*, **6**(4), 439-455.
Zurn Ind. (1977), "Design blue lines and copies: shell reinforcing - tower 1 & 2", Grand Gulf Nuclear Station, Nov. Provided by private comm. from Zurn Balcke-Durr Ind., Inc., Tampa, FL.